Arabian Journal for Science and Engineering (2019) 44:7173–7185
https://doi.org/10.1007/s13369-019-03842-6

RESEARCH ARTICLE - ELECTRICAL ENGINEERING

Real-Time Simulation of Smart DC Microgrid with Decentralized Control System Under Source Disturbances

Ginbar Ensermu[1] · **Avik Bhattacharya**[1] · **Nigamananda Panigrahy**[2]

Received: 10 December 2018 / Accepted: 1 April 2019 / Published online: 23 April 2019

Abstract
Decentralized control of DC microgrid (dcμG) using hybrid renewable energy sources (RES) and battery energy storage system (BESS) which operate with and without grid-connected mode is proposed in this paper. In dcμG integrated with multiple RES and BESS, fluctuating output characteristics of the distributed generations (DGs) due to changing input conditions and the dynamic interactions of the source and load interface converters are main factors which cause stability problem of DC bus voltage. Thus, to solve this problem, the decentralized control scheme which uses bus voltage level as communication link in the control law is proposed in this paper. Accordingly, the control method realizes different operating modes based on the available generations and load demand. Maximum power and constant voltage controls schemes are applied in the DGs interfacing control to regulate the power and voltage variations due to changing input conditions. Furthermore, in the control strategy, the source and battery interfacing converters are controlled autonomously using the bus voltage level without any communication. This maintains the reliability and flexibility of the system. The proposed system model is developed with Matlab/Simulink SimPowerSystem and simulated with real-time simulation using OPAL-RT.

Keywords Constant voltage control · DC microgrid · MPPT control · Real-time simulation · Renewable energy resource

1 Introduction

With the advancements in power electronic technologies, the penetration of DGs with energy storage system is increasing in the modern distribution power network [1, 2]. DGs are the small-scale power generation system comprising of renewable energy resources and conventional energy generation units [2, 3]. The direct interconnection of hybrid multiple distributed energy resources (DERs) such as wind turbine, photovoltaic (PV), and battery energy storage units with AC grid supply causes problems of frequency and voltage control within the system [2, 4, 5]. Accordingly, to overcome the aforementioned problems, microgrid concept was introduced to enable the integration of AC grid, DGs, ESSes, and loads through power electronic interface converters [3, 6], and the electrical parameters such as voltage, power and frequency variations are regulated through these converters. Microgrids can be classified as AC, DC, or AC/DC hybrid based on the voltage and current types. Depending on the operation system, it can be also divided into two: grid-connected and islanded microgrids [7]. Most energy sources such as solar PV, fuel cell and battery energy system are generating DC in nature. Nowadays, also DC-operated electronic loads are developing that eliminate further power conversion stages which reduce cost and losses. In addition, in DC system reactive power control, synchronization technique and frequency control do not exist [8, 9]. Thus, the dcμG is more advantageous than its AC counterparts.

In recent years, wind and solar distributed generations are becoming the most popular distributed renewable energy sources for microgrid applications. A hybrid wind and PV system with grid-connected system provides more reliability and higher quality power to the load than a system with single source in microgrid system [10]. In such a system, the power electronic interfacing converters are used for integrating the different DERs and regulate the voltage, frequency,

✉ Ginbar Ensermu
ginbalem@gmail.com

Avik Bhattacharya
avik.iitkgp@gmail.com

Nigamananda Panigrahy
Nigamananda.Panigrahy@opal-rt.com

[1] Department of Electrical Engineering, IIT Roorkee, Roorkee 247667, India

[2] OPAL-RT Technologies India Pvt Ltd, Delhi, India

and power between the source and load subsystems. The increasing number of RES penetrations in the recent distribution network and the increased consumer energy demands from a nearby site, encouraged the deployment of dcμG with multiple sources and energy storage opportunities so as to deal with the control, reliability, and stability problem in the integrated systems [11, 12, 13]. When a dcμG is interfaced with different sources in parallel, each source in the system participates with supporting each other via an integrated and power management control strategies. Consequently, this can provide various benefits such as optimal operation of dcμG subsystem through coordinated control scheme that maximize utilization of DGs and BESS [11, 14] and maintain the reliability and power balance of the dcμG in case of generation and load disturbances [12, 13]. The fluctuating output characteristics of DGs, the dynamic interaction between source and load interfacing converters, and a sudden load changing are the main causes of stability problems of bus voltage in microgrid system with various sources integrated [10]. Therefore, to realize reliable and flexible operation in a dcμG with various electronically coupled sources different control techniques are proposed in [11, 15, 16]. A distributed control method is proposed in [11] for multiple parallel interconnected sources of islanded dcμG. In the proposed system, a coordinated control employing a typical droop control is applied. A droop control method is proposed for appropriate load sharing among various DC converters in [17, 18]. In order to decrease the circulating currents between different sources, coordinated voltage controller is implemented in [9, 10]. In [19], a centralized control technique is presented to interface the operation of different converters in dcμG which are connected in parallel.

This control strategy used the model predictive control scheme for power sharing and voltage control. But, this control mechanism degrades the system reliability and flexibility, and it is more susceptible to failure with a single-point fault in the system. A master–slave control method for load sharing is proposed in [20]. However, this control solution also have similar problem with the centralized control in which the failure of master–slave causes failure in voltage regulation. In [9], distributed control scheme which operates with droop control that can facilitate maximum load transfer to load using fuzzy logic controller is proposed. But this control system has the drawbacks of complex computational analysis, slow communication, and vulnerability to measurement error [9]. Many studies reported in [10, 21] proposed control of energy management methods primarily on islanded dcμG by optimized usage of RES and ESS. However, such control approaches may lead to poor reliability and create more burdens on ESS due to the intermittent behavior of the solar insolation and wind speed [8, 10]. A decentralized control structure is reported in [5, 22], with multiple dcμG sources. This control system enables to perform local control functions in each source converters to realize the voltage and power regulation. In addition, every power converters in the system employed independent control without any communication link between different units. Thus, for effective and reliable operation of dcμG, a suitable integrated control strategy is required.

In this paper, coordinated decentralized control strategy among the various sources and loads is proposed. A dcμG composed of wind–solar hybrid RES and BESS with grid-connected or islanded operations that allow flexible and reliable performance with seamless mode transition is presented. The proposed control system employs the DC bus voltage level as a reference signal, and it is implemented with autonomously controlled source units in order to stabilize the DC bus voltage variations due to the fluctuating behavior of the wind speed and solar insolation of RES and sudden load changing. Moreover, system realizes the optimal operation of the dcμG by maximizing the distributed generations with voltage and maximum power control mode in relation to the decrease/increase in load demand, maintaining economical operation of ESS and regulating the bus voltage within the particular margins. The developed dcμG control is implemented in real-time simulations with control-in-the-loop (CIL) to verify the controller accuracy and performance. Accordingly, the dcμG system model and controller design are applied to the simulator to test the system controller and operation performances. The proposed CIL simulation is implemented in OPAL-RT with RT-LAB real-time simulation environment. The remaining of paper is organized in the following sections. In Sect. 2 the proposed dcμG configuration and working principle are elaborated. The system control scheme is detailed in Sect. 3, and in Sect. 4 the general concept of the real-time simulation is described. The developed dcμG model results are explained in Sect. 5. Finally, Sect. 6 summarizes the work with conclusion.

2 The Proposed System Configuration and Operating Mode Algorithms

2.1 Configuration of Proposed DC Microgrid

The proposed dcμG in this paper is portrayed in Fig. 1. The system comprised of G-VSC, wind–solar hybrid RES, BESS, and DC loads. Each source unit in the system is interfaced to the main DC bus through power electronic interfacing converters. In the proposed system, AC grid supply is interfaced to the DC bus through three-phase voltage source converter (VSC). This converter is used due to its ability to achieve a sinusoidal input current with THD less than 5% by utilizing pulse width modulation techniques in combination with the inner current control loop as shown in Fig. 2a.

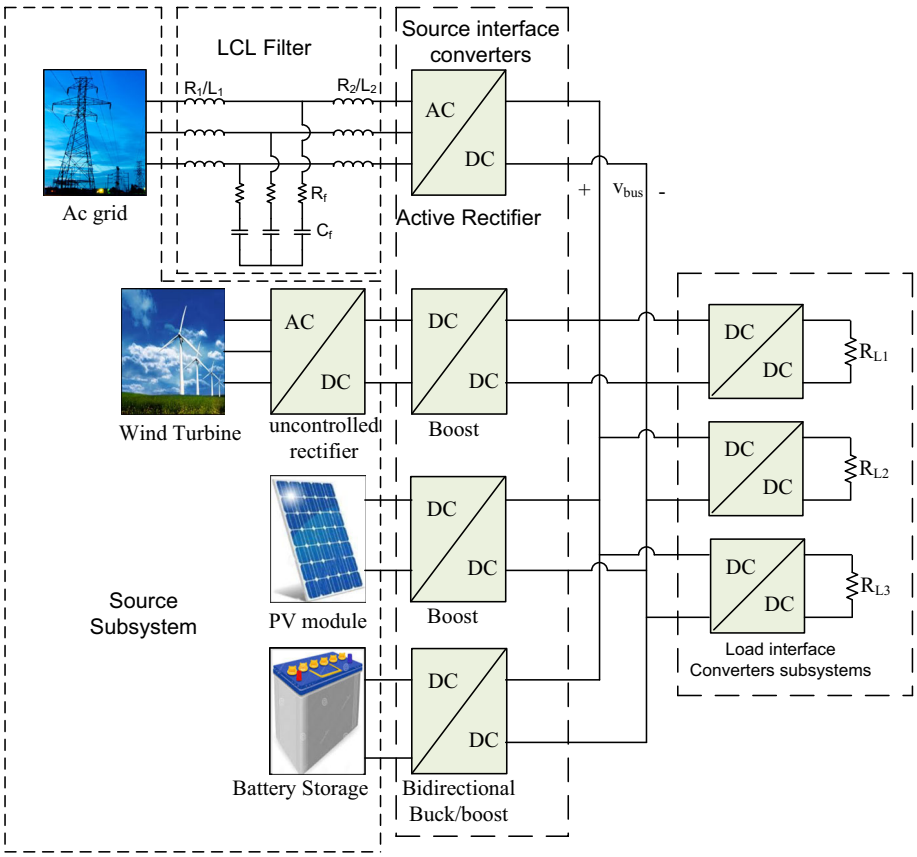

Fig. 1 Proposed DC microgrid configuration

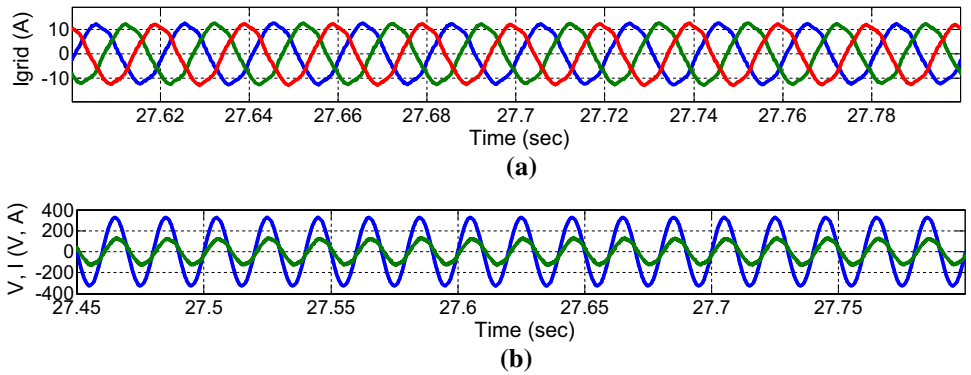

Fig. 2 Grid input parameters: **a** input three-phase current and **b** phase-to-neutral voltage and line current (10 times increased)

Moreover, the converter enables to achieve unit power by controlling the grid voltage and current as illustrated in Fig. 2b. The high-order harmonic frequencies which are created by nonlinear switching operation of VSC can be also attenuated by employing LCL filter on the input side of the converter. Further, the converter has full potential to control both the power flow and DC link voltage [23]. The renewable generation sources are interleaved to main bus via the boost DC/DC converter. The wind subsystem uses PMSG to generator variable three-phase AC voltage. This variable generated voltage applied to three-phase uncontrolled rectifier to convert it to DC voltage and supply to the boost converter [24]. Similarly, variable DC voltage generated by the PV modules is fed to the boost converter. In both cases, the boost DC/DC converter performs two functions: (1) track maximum power from both wind and PV and boost the generated voltage to the level desired by DC bus, (2) it facilitates capturing of maximum power from the DGs with the changing input environmental conditions. In this paper, perturb and observe (P&O) MPPT scheme is implemented for maximum power point tracking control [25].

The battery energy storage system is integrated to the common DC bus through bidirectional buck/boost DC/DC converter. The converter also used to control the operating characteristics of the battery and regulate the power variations on the DC bus. The converter employed two PI

Table 1 Power flow operation at various operating modes

Operating modes	dcμG operation type	Power flow VSC	Power flow battery
DG	Islanded	$P_{grid} = 0$	$P_{bat} < 0$
G-VSC	Grid connected	$P_{grid} > 0$	$P_{bat} < 0$
BESS	Islanded	$P_{grid} = 0$	$P_{bat} > 0$

controllers in the voltage control loop for charging and discharging operations. In boost mode, the detected and the reference DC bus voltages are compared to generate input signal for one of the PI controller for discharging control. However, the difference of measured battery and its reference voltage are compared to produce input signal for the other PI controller (in buck mode) for charging control. In both cases, the controllers are employed to generate a battery reference current that provide a desired signal for inner current controller to generate pulse signal to control the converter duty ratio [1].

2.2 Proposed dcμG Operating System

The common DC bus voltage is used as a communication signal for mode transitions among the operating modes. In practice for power balancing at the DC bus, there are many different interconnecting control problems such as effective usage of energy storage system, exploiting DGs power production and regulating bus voltage within the particular margin [10].

In dcμG with multiple microsources, the optimized operation can be realized through decentralized control using DC bus signaling control scheme. This control method realizes the adaptive mode transition among the different operating modes [17, 22]. Thus, the decentralized control approach based on bus voltage level is implemented to regulate the proper function of the dcμG system under varying input conditions.

The intended objective is to regulate the power flow among the autonomously controlled sources and storage unit and maintain the stability of DC bus voltage within a particular range. The power flow at the various mode of operation is presented in Table 1. Thus, the operation of the hybrid dcμG proposed in this paper is categorized into three operating modes as shown in Fig. 3.

2.2.1 Distributed Generation Mode

Figure 3a shows DGs mode of operation. In this mode, the dcμG works in islanded mode. During this mode, the load power is less than the generation power. Due to light load demand, the bus voltage increase to the maximum limit and the bus voltage operating in the range of $1.025V_{dcn} < v_{busref} < 1.05V_{dcn}$. The excess power from the DGs during this period is supplied to the battery for charging. The DGs converter shifts from MPPT control to constant voltage control to regulate the bus voltage. In this mode, AC grid is disconnected and the battery interfacing converter regulates the bus by absorbing the excess power.

2.2.2 Grid-Connected Mode

The three-phase VSC is used to connect AC grid with common bus. This converter is used to regulate voltage, current and harmonics due to converter's nonlinear switching operations. In this paper, grid-connected system is established to balance the power deficient due to lack of generations from DGs to satisfy the load demand by exporting power to the DC bus. In this mode, the VSC assumed as a voltage source and the operating mode is shown in Fig. 3b. The DGs converter during this mode operates at MPPT control. The battery energy system works in charging operation. During this mode, the operating bus voltage is between the range of $0.975V_{dcn} < v_{busref} < 1.025V_{dcn}$, where V_{dcn} is nominal DC bus voltage and v_{busref} is the reference bus voltage.

2.2.3 Battery Storage Mode

This operating mode is portrayed in Fig. 3c. The dcμG is disconnected from grid; however, the load power is greater than the generation power. Thus, since generation is less than load power, the battery regulating the DC bus power balances by discharging, and hence, it works as a voltage source. The DGs are working in MPPT control. During this time, the bus voltage is decreased due to load power is increased, and it is operating between the range $0.95V_{dcn} < v_{busref} < 0.975V_{dcn}$.

3 Proposed System Control

3.1 Grid-Connected Voltage Source Converter System and Its Control Method

In this paper, a G-VSC with rectifier operation mode is used for power transfer from AC system to a DC bus. In Fig. 6, R_{Line} and L_{Line} represent the line resistance and inductance between converter voltage (V_{conv}) and AC grid voltage (V_s), respectively. V_{sabc} and i_{sabc} are grid voltage and current, respectively. The capacitance C_{dc} is employed to smooth DC link voltage (V_{dc}). When a G-VSC is integrated with DG to form a common DC bus, problems such as line notching, voltage unbalance, and frequency variations may exist. Accordingly, in this paper, to overcome the aforementioned problems, two main control systems are employed, namely phase-locked loop (PLL) and vector control systems.

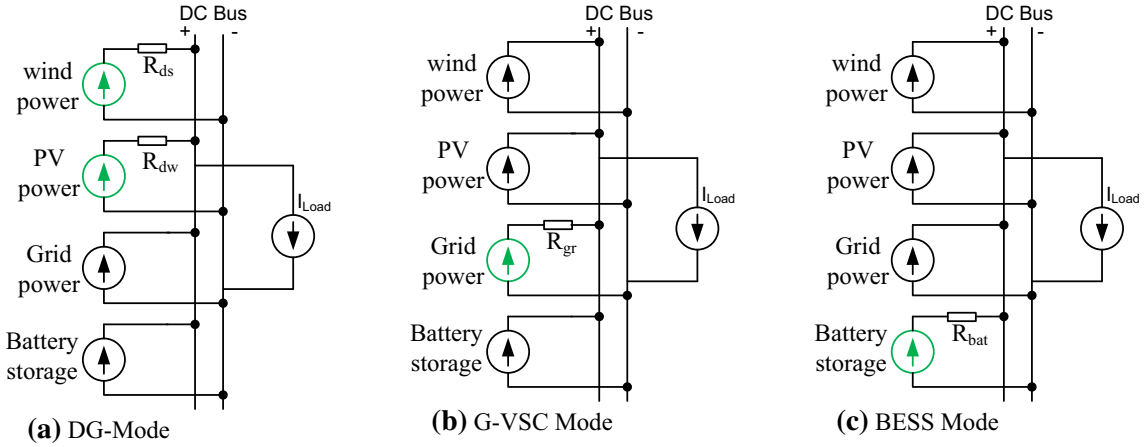

Fig. 3 Operating mode definitions [11]

3.1.1 Phase-Locked Loop (PLL) Control

The grid side voltage V_{sa}, V_{sb} and V_{sc} is sensed and converted to stationary reference frame V_α and V_β, and this stationary frame is further converted to synchronously rotating reference frame (SRF) V_{sq} and V_{sd}. When G-VSC operates in rectifier operation mode, the voltage vector $\bar{V}_s$ is aligned with q - axis and the d - axis lags the q - axis by 90° [26]. Assuming a balanced three-phase AC supply, a SRF–PLL control method is developed based on the following mathematical analysis:

$$\begin{bmatrix} V_{sa} \\ V_{sb} \\ V_{sc} \end{bmatrix} = \begin{bmatrix} V_m \cos\theta \\ V_m \cos\left(\theta - \frac{2\pi}{3}\right) \\ V_m \cos\left(\theta - \frac{4\pi}{3}\right) \end{bmatrix} \tag{1}$$

$$\begin{bmatrix} V_\alpha \\ V_\beta \end{bmatrix} = \begin{bmatrix} V_{sa} \\ \frac{(V_{sc} - V_{sb})}{\sqrt{3}} \end{bmatrix} \tag{2}$$

$$\begin{bmatrix} V_{sq} \\ V_{sd} \end{bmatrix} = \begin{bmatrix} -\sin\theta^* & \cos\theta^* \\ \cos\theta^* & \sin\theta^* \end{bmatrix} \begin{bmatrix} V_\alpha \\ V_\beta \end{bmatrix} \tag{3}$$

where V_m is the phase-to-neutral amplitude voltage. Substituting (1) and (2), into (3), the voltage V_{qe} and V_{de} is obtained as [17]:

$$\begin{bmatrix} V_{qe} \\ V_{de} \end{bmatrix} = \begin{bmatrix} \cos(\theta^* - \theta) \\ \sin(\theta^* - \theta) \end{bmatrix} = \begin{bmatrix} \cos(\Delta\theta) \\ \sin(\Delta\theta) \end{bmatrix} \tag{4}$$

The control scheme is illustrated in Fig. 4 and as shown in the figure PI controller is employed to achieve the value of ω^* that determines the feedback voltage V_{de}^*. Thus it should be noted that if the difference in angle $(\Delta\theta)$ between the PLL output θ^* and grid angle θ is kept zero, then $V_{qe} = V_m$ and $V_{de} = 0$ as presented in Fig. 5. The angle used in the transformation system is obtained by integrating a reference frequency ω^*. If the resulting command frequency is similar to the AC grid frequency, the voltages V_{qe} and V_{de} regarded

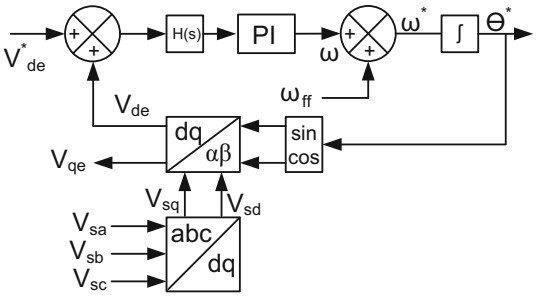

Fig. 4 PLL control block

as DC values based on the angle θ^*. Accordingly, the phase difference between $\sin(\theta^*)$ or $\cos(\theta^*)$ and grid voltage is determined by the voltage magnitude of V_{de}. $H(s)$ shown in Fig. 4 represents lead compensator transfer function, and it is used to attenuate the harmonic distortion of the three-phase grid line voltages [27].

3.1.2 VSC Voltage and Current Control

The control strategy is carried out via synchronously rotating $d-q$ reference frame [26]. Thus the transformed grid side voltage and line currents are used as feedback parameters for the inner current control loop as shown in Fig. 6. The outer voltage controller is employed to regulate the DC voltage and sets the reference input for the q-axis current controller. The active power is regulated through the inner q-axis current control loop, while reactive power is controlled via d-axis current loop due to i_{sq} is a measure of P_s, and similarly, y is the measure of Q_s as shown in (5) [26]. Using the power invariant transformation, the total instantaneous active and reactive power in dq frame is given by:

$$P_s = \frac{3}{2}\left(v_{sq} i_{sq} + v_{sd} i_{sd}\right) = \frac{3}{2}\left(v_{sq} i_{sq}\right) \tag{5a}$$

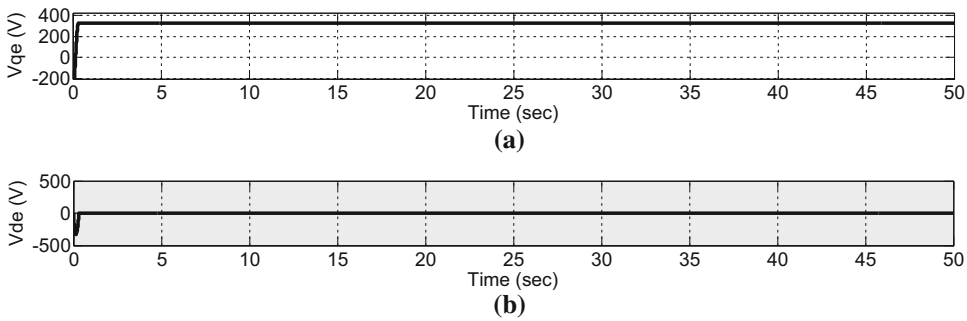

Fig. 5 DQ-axis voltage, **a** q-axis voltage, **b** d-axis voltage

$$Q_s = \frac{3}{2}\left(v_{sq}i_{sd} - v_{sd}i_{sq}\right) = \frac{3}{2}\left(v_{sq}i_{sd}\right) \tag{5b}$$

where P_s is the active power and Q_s is the reactive power. The feed-forward terms $\omega L i_{sq}$ and $-\omega L i_{sd}$ are combined with the inner current control system to allow effective decoupled control of the i_{sq} and i_{sd}.

3.2 Wind and Solar Boost Converter Control

In RES system, parameters such as input disturbances (change in irradiation and wind speed), loads demand, and the status of other sources in the microgrid determine the operating modes of DG systems. Accordingly, the control system for DGs source can be categorized into two. These are constant voltage and MPPT control as illustrated in Fig. 7. In Fig. 7, V_{pv}/V_w represent converter primary side voltage, I_{pv}/I_w represents converter input current, respectively. V_{dc} and I_{dc} are converter output voltage and current, respectively. The converter input voltage is sensed and compared with its reference value and the error generated is applied to the voltage controller to regulate the converters input voltage through the closed loop. During light load, when there is sufficient DG generation is available, the DG converters are controlled to operate at constant voltage control (CVC) mode to smooth bus voltage.

In this case, the DC bus voltage increases due to less load power and the switch control logic will change to CVC mode. However, when different converters are connected in parallel, there will be a circulating current among the converters. Thus, in order to overcome, this problem, a droop control is used to suppress the circulating current [10, 18, 22]. In mode-II, due to increase in load power, G-VSC is connected to the dcμG to supply the deficit power for the load. The DG boost converters are working at MPPT control and the control logic switches to MPPT mode in Fig. 7. During this period, generation power is increased while the DC bus voltage is decreased. As a result, DGs are controlled to operate at maximum power point (MPP) in order to maximize the available energy.

3.3 Battery Converter Control System

In mode-I, since DG power is greater than load demand, the bidirectional buck/boost converter works in buck mode to charge the battery and regulate the DC bus by absorbing the extra power. It is assumed that the battery is fully charged when its state of charge is reached 95% and depth of discharge is 40% [28]. Accordingly, in this mode, if the battery is not fully charged, it continues to be charged in mode-II.

The schematic control block diagram for battery control proposed in this paper is shown in Fig. 8, where V_{bat} and V_{batref} represent the measured and desired battery voltages, V_{bat_L} is the battery voltage at 40% SoC, I^*_{bat} is battery reference current, I_{bat} the measured battery current. The battery charging and discharging status is determined by I^*_{bat}, which is the summation of charging and discharging battery output current ($I_{k1} + I_{k2}$) as shown in Fig. 8. Moreover, when $I^*_{bat} > 0$, the bidirectional DC/DC converter works in boost mode, and hence, the battery is discharging to regulate the DC bus power balance (during mode-III), while $I^*_{bat} < 0$ battery is in charging mode. Thus the seamless transition among the various modes is ensured [28].

3.4 Analysis of Droop-Controlled Source Converters

Droop control allows source converters to operate in parallel, so that loads can be shared among the generating sources in proportion to their power rating. When the droop resistance R_d is connected in series with Thevenin voltage (V_{Th}), the reference bus voltage is given by

$$V_{busref} = V_n - R_d i_o \tag{6}$$

The droop resistance can be found by:

$$R_d = \frac{\Delta v_{bus}}{i_{max}} \tag{7}$$

When the microsources in DC microgrid work in voltage droop mode, each source in the system is accountable to make

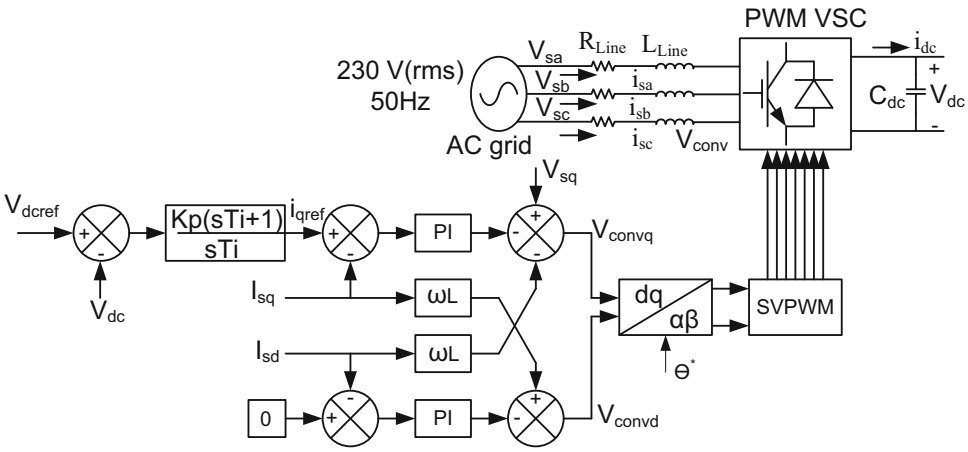

Fig. 6 VSC control system

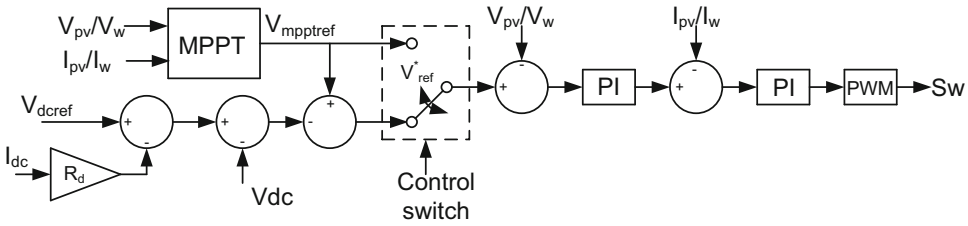

Fig. 7 Wind and PV boost DC/DC converter control

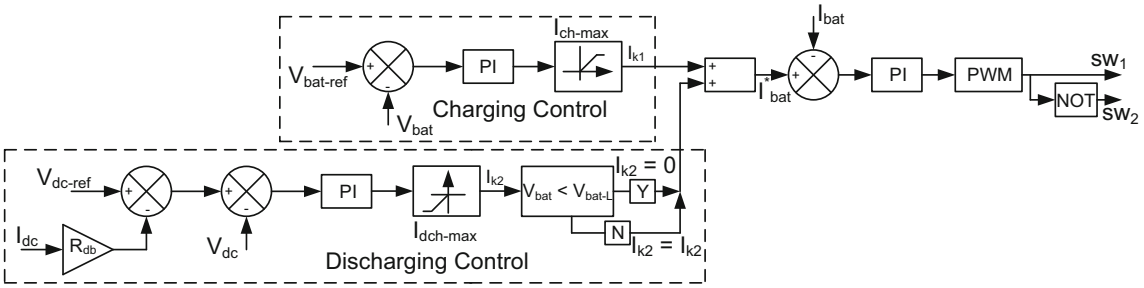

Fig. 8 Battery BDC control block

the bus voltage stable, so that the current at each terminal converter is given by [29]:

$$i_s = i_1 + i_2 + i_3 + i_4 \tag{8}$$

Considering that all sources have the same reference voltage when controlled in constant voltage control [30], the reference bus voltage can be calculated as:

$$V_{\text{busref}} = V_n - \frac{1}{\sum_{i=1}^{n} \frac{1}{R_{di}} i_s} = V_n - R_d i_o \tag{9}$$

The difference between powers delivered from parallel sources can be realized by analyzing power to a given load with simplified circuit of the two sources. The dcμG source components are listed in Table 2. The equivalent steady-state analysis of the simplified circuit can be done by modeling source units as voltage source in series with droop impedance, as depicted in Fig. 9. Thus the change of current delivered by source is obtained as:

$$I_1 - I_2 = \frac{2(V_1 - V_2)}{R_{d1} + R_{d2}} + \frac{(R_{d1} - R_{d2})}{R_{d1} + R_{d2}} I_0 \tag{10}$$

$$V_{\text{bus}} = V_{\text{Th}} - R_d I_0 \tag{11}$$

where $V_{\text{Th}} = \frac{V_1 R_{d2} + V_2 R_{d1}}{R_{d1} + R_{d2}}$ and $R_d = \frac{R_{d1} R_{d2}}{R_{d1} + R_{d2}}$

Equations (10) and (11) show that the change in current delivered by each generating unit is inversely proportional to the sum of droop resistances as shown in (10). Consequently, as the total droop resistances increased, this decreases the difference between currents. However, increasing droop resistances leads to poor voltage regulation. Thus, there must be a trade-off between load sharing and voltage regulation [30].

Table 2 dcμG components design parameter

Units	Types of interfacing converter	Rated power (kW)	Droop resistance (Ω)
Wind turbine	Boost converter (nonisolated)	6	3.23
PV Module	Boost converter (nonisolated)	12	0.91
AC grid	Three-phase VSC	5	4.02
Battery (ESS)	Bidirectional buck/boost	5	2.01

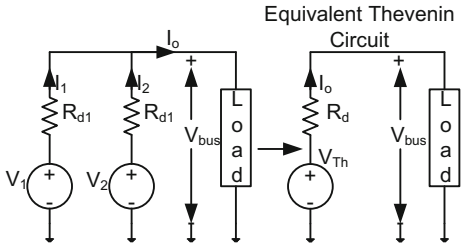

Fig. 9 Simplified equivalent circuit for two sources connected in parallel supplying a load and its Thevenin equivalent [27]

3.5 Control of Load Interface Converter

The voltage mode control method is employed in this paper for load converter, and compensator parameters are designed based on frequency control. In Fig. 10a, the converter output voltage V_o is sensed and compared with reference voltage V_{ref} and generate an error signal. The intended objective is to achieve the output voltage equal to V_{ref} such that the average output voltage follows the desired input voltage regardless of disturbances in converter power stage. In the control strategy, if the feedback system works accurately, then reference input signal matches with the output voltage and hence the error signal is zero [31].

3.6 System Stability Analysis

In actual practice, the load interfacing converter injects a pulsating current into the power stage. This current contains a high-order harmonic at multiples of the switching frequency (f_{sw}) which can affect the current spikes caused by switching transitions. Moreover, the input source voltage transient also causes conducted audio susceptibilities [31, 32]. Therefore, in order to overcome the aforementioned problems, an input filter is employed at the input converter terminals. The input filter is used to attenuate disturbances due to switching devices and also limit the conducted electromagnetic interference (EMI). The stability problem of the system can be improved using parallel passive input filter with an optimum damping at the converters input terminals as depicted in Fig. 10b. The optimum value of damping resistance (R_d) can be obtained at the minimum value of filter output impedance (Z_o). When the damped filter is combined with the negative converter input resistance, the resultant effect is positive. The value of this damping resistance can be approximated using the filter peak output impedance as given in (12) [32]:

$$|Z_o|_{max} = R_o \frac{\sqrt{2(2+n)}}{n} \tag{12}$$

where $R_o = \sqrt{\frac{L_f}{C_f}}$. The value R_d can be found using the following expression:

$$R_d = R_o \sqrt{\frac{(2+n)(4+3n)}{2n^2(4+n)}} \tag{13}$$

The control to output open-loop transfer function ($G_{vd}(s)$) of load converter shown in Fig. 10b with damped input filter can be expressed as [32]:

$$G_{vd}(s) = V_g \frac{s^3 a_3 + s^2 a_2 + s a_1 + 1}{s^5 b_5 + s^4 b_4 + s^3 b_3 + s^2 b_2 + s b_1 + b_0} \tag{14}$$

where the numerator and denominator are given in the following

$$a_0 = 1,\ a_1 = nC_f R_d - D^2 L_f / R$$

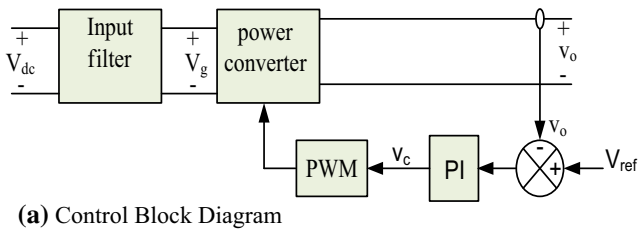

(a) Control Block Diagram

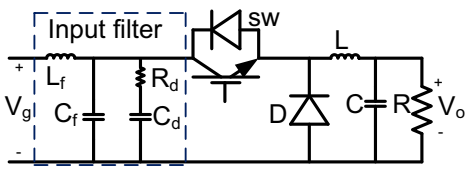

(b) Circuit Diagram

Fig. 10 Buck converter with damped input filter

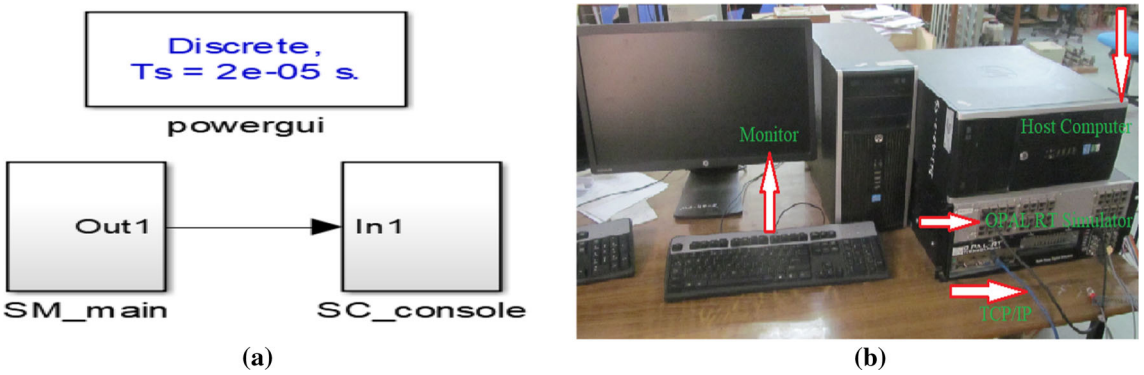

(a) (b)

Fig. 11 Real-time simulation setup using OPAL RT simulator: **a** Simulink model using RT LAB and **b** simulator setup picture

Table 3 Bus voltages at different operating modes

DG-mode (V)	G-VSC mode (V)	BESS mode (V)
≥ 665	≥ 650	≥ 634

$$a_2 = L_f C_f\left(1+n-\frac{nD^2L_f}{R}\right),\ a_3 = nL_fC_f^2R_d$$
$$b_0 = 1,\ b_1 = nC_fR_d + \left(L + D^2L_f\right)/R$$
$$b_2 = C\left(D^2L_f + L\right) + L_fC_f + nL_fC_f + nC_fR_d\left(L + D^2L_f\right)R$$
$$b_3 = \frac{L_fC_fL(1+n)}{R} + nC_fR_d\left(L_fC_f + LC + D^2L_fC\right)$$
$$b_4 = L_fC_fLC(1+n) + nL_fLR_dC_f^2/R$$
$$b_5 = nL_fC_f^2LCR_d$$

The addition of input filter at converter input terminal degrades the stability of the closed-loop control. The input filter introduces complex poles and zero on the right half plane which causes system instability. In this paper, the Routh–Hurwitz criterion is used to find the stability conditions from the closed-loop characteristic equation $(1 + G_{vd}(s))$. Accordingly, the following two conditions determine when the real signs of zero and poles are negative.

$$L_fC_f(1+n) - \frac{nL_fD^2R_d}{R} > 0 \tag{15}$$

$$\frac{D^2L_fC_f^2(1+n)}{R} - nL_fC_f\left(D^4L_f + nC_f\right)R_d + \frac{n^2D^2C_f^2}{R}R_d^2 > 0 \tag{16}$$

By selecting optimum values of R_d and C_d where $C_d = nC_f$, the stability of the closed loop can be analyzed using open-loop transfer function.

4 Concept of the Real-Time Simulator

Real-time simulations are important to verify the controller performance and accuracy since models developed in real-time are executed at the same rate with actual physical system. The OPAL-RT simulator interacts with Matlab/Simulink SimPowerSystem through RT-LAB software. The key purpose of the simulator is to implement real-time, HIL, and control-in-the-loop (CIL) simulations. In this paper, the developed dcμG model with Simulink using SimPowerSystems is realized in real-time simulation using ARTEMiS-SSN solver. This solver is used to decouple large power systems state space into smaller groups, whose solutions can be obtained simultaneously by using a nodal admittance method. In addition, it provides fast and accurate real-time simulation of dcμG systems using the most advanced processors. The ARTEMiS-SSN performs parallel execution by assigning multiple cores per CPU for computations of subsystems that contains several state-space nodal (SSN) groups. The dcμG system shown in Fig. 1 consists of large electrical components (such as grid source, wind turbine generator, solar PV array and battery blocks) and smaller power electronic components (such as switches and breakers). Decoupling the large electrical components into smaller electrical components with ARTEMiS-SSN, the proposed dcμG is simulated at a time step of 20 μs on 2.8 cores, 3.2 GHz processor speed, and 16 GB RAM RT-LAB simulator.

Finally, the parallel tasks can be built from Simulink model using RT-LAB, and each task assigned on the processor of the multicore computer and the whole simulation can be run [33, 34]. The dcμG model simulation setup via OPAL-RT digital simulator is presented in Fig. 11.

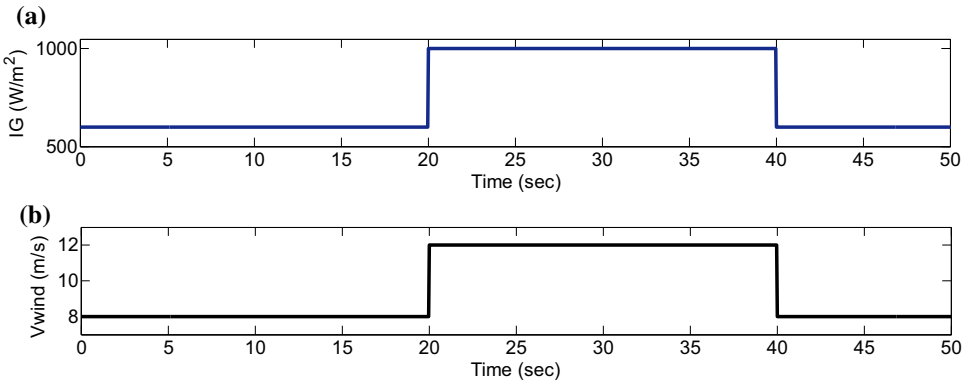

Fig. 12 DGs inputs, **a** irradiation, **b** wind speed (m/s)

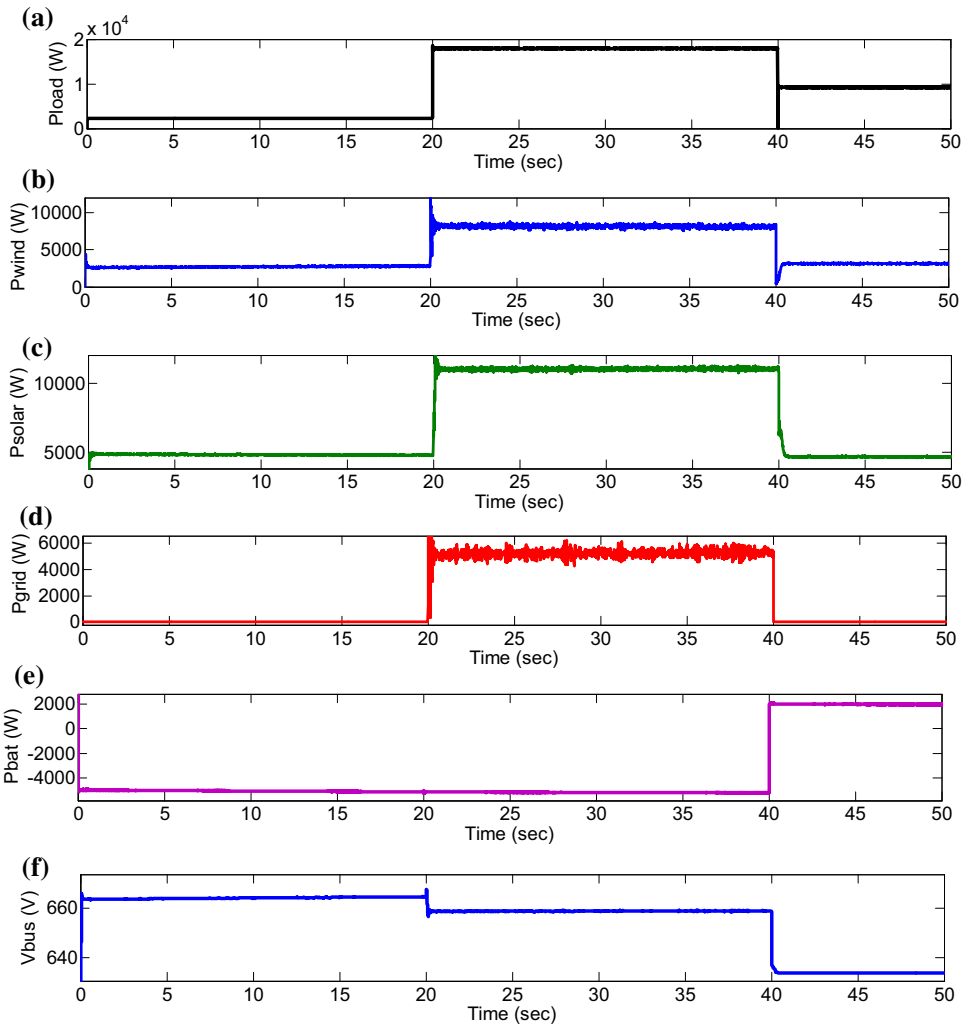

Fig. 13 Proposed system real-time simulation: **a** load power, **b** wind power, **c** solar power, **d** grid power, **e** battery power, and **f** DC bus voltage

5 Results and Discussion

To evaluate the effectiveness of the proposed control strategy, the proposed system model has been developed in Matlab/Simulink, and with some modification, it is simulated using OPAL-RT, RT-LAB real-time simulation environment. The simulation is done with fixed step and sample time of 20 μsec. As it is described in Fig. 1, the proposed architecture comprises G-VSC, PV module, and wind turbine interfaced to DC grid via boost DC/DC converter, BESS which is linked to main DC grid via bidirectional buck/boost, and DC loads which are supplied power from the common DC bus through buck interface converter. The DC bus voltages values at the different modes are listed in Table 3. A

Table 4 System parameter

Source units	Parameters	Values	Units
Wind	Power rated	7	kW
	Sw. frequency	5	kHz
	Rectified DC voltage	400	V
Solar	Power rated	12	kW
	Sw. frequency	5	kHz
	PV Module Voltage	300	V
G-VSC	Power rated	5	kW
	Sw. frequency	5	kHz
	Rectified DC voltage	650	V
BESS	Battery Voltage	240	V
	Sw. frequency	5	kHz
	Power rated	5	kW
Load	Power	2.24–18	kW

sudden change in input disturbance is employed using step signal for PV and wind turbine source units as shown in Fig. 12. The constant power control and constant voltage control of DGs are realized via the boost converter for DGs sources. Figure 13 shows the real-time simulation results of the proposed system. The system design values used in the simulation are listed in Table 4. To verify the control performance, the microsources and load are programmed to change mode transitions between the various modes.

The load power change is shown in Fig. 13a. Figure 13b, c depicts the power supply variation from wind and PV generations, respectively. The variations in power from G-VSC and BESS units, which are required to satisfying the load demand, are illustrated in Fig. 13d, e, respectively. Similarly, the variation in bus voltage level is depicted in Fig. 13f. During the time duration $t = 0$–20 s, the power generations from wind and PV are 2.5 kW and 5 kW, respectively, which is depicted in Fig. 13b, c. However, the load demand is 2.5 kW which is less than the sum of DGs power as shown in Fig. 13a. At this period, the dcμG is in islanding mode with generation from DGs is greater than the power required by load. As a result, the surplus power from DGs is charging the battery, and in this mode, battery is regulating the bus by absorbing the extra power. At $t = 20.01$–40 s, the load power is increased to 19 kW as shown in Fig. 13a, and BESS is also charging with 5 kW shown in Fig. 13e. In this duration, the DGs power is less than the total demanded power. Thus, to compensate the deficit, G-VSC is connected to supply 5 kW power as illustrated in Fig. 13d. In this mode, G-VSC is regulating the bus by delivering the deficient power for the load. In the duration $t = 40.01$–50 s, the G-VSC is disconnected and the power generation from DG is also decreased from 18 to 8 kW (PV power is 4.4 kW and wind power is 3.6 kW). At this time, the load power is 9 kW as demonstrated in Fig. 13a, which is greater than generation capacity. Thus, the BESS changes operation to discharging mode to fulfill the power mismatch. Accordingly, the BESS discharges 2 kW power to maintain the power balances on the DC bus which is depicted in Fig. 13e. The result obtained by real-time simulation verifies that the successfulness of the proposed control. The input disturbances employed to the proposed system in this paper caused mode transitions automatically among the microsources to regulate the power management in the system.

Stability of the closed loop of point of load converter is investigated from the open-loop transfer function, $G_{\mathrm{vd}}(s)$. In a well-designed input filter with optimum damping parameters, the source output impedance (Z_{o}) will become sufficiently small. This result in the impact of input filter on the closed-loop control system becomes negligible. Accordingly, the converter control works properly with better performance. In this paper, with the following converter parameters, Nyquist stability criteria are tested: $L_{\mathrm{f}} = 1.8$ mH, $C_{\mathrm{f}} = 1$ mF, $n = 4$, $R_{\mathrm{d}} = 0.78$, $L = 1.3$ mH, $C = 25$ μF, $D = 0.49$ and $R = 21$ Ω. Figure 14a shows the frequency bode plot of the converter open-loop transfer function with and without input filter addition. As can be seen from the figure with a well-damped input filter, the control system performance cannot be affected. The Nyquist diagram without and with input filter is also shown in Fig. 14b, c, respectively, which shows that in both plots the result is similar. Thus, this shows that the system is stable.

6 Conclusion

In this paper, dcμG with multiple renewable energy sources and energy storage system is presented using the decentralized control structure. The control solution is fully based on the independent control operation of source converters based on the bus voltage levels as a communication link that enables various operating modes depending on the generating source conditions. In addition, the control technique employed voltage and power control modes to regulate the voltage and power oscillations which are caused by the changing input conditions. Considering the generation output and sudden load changing impacts, three modes of operations are implemented in this paper in order to maintain the system reliability and flexible operations. The operating mode characteristics of the proposed system are explained based on bus voltage level that allows smooth mode transitions and reliable load sharing. To improve the source transients of the system, a low-pass passive filter is designed with parallel damping. The detail model of the proposed dcμG is developed in Matlab/Simulink SimPowerSystem and also simulated with real time using OPAL-RT with small modifications. Thus, this

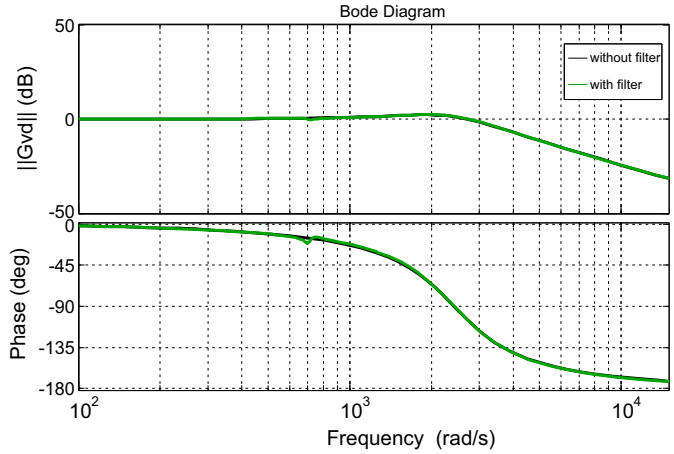

(a) Bode plot with damped filter and without filter

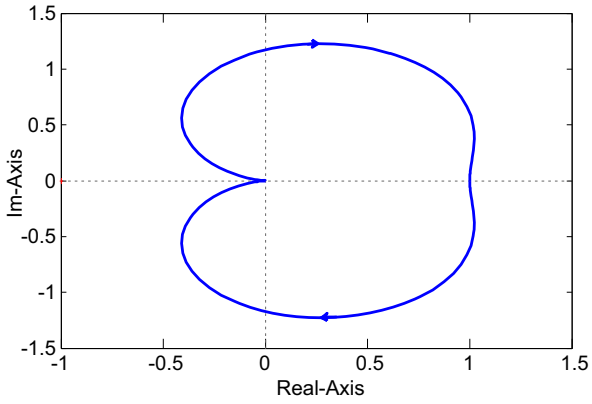

(b) Nyquist Plot without filter

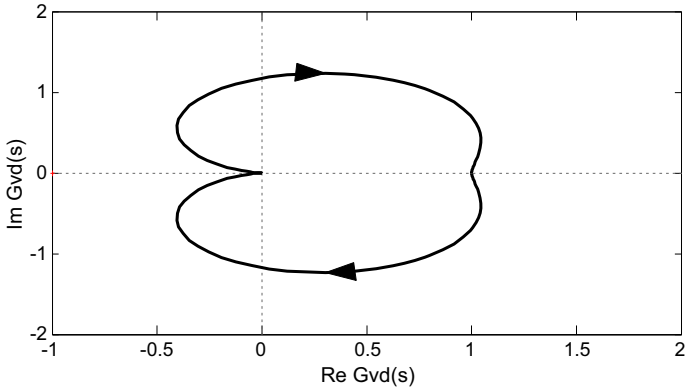

(c) Nyquist Plot Without input

Fig. 14 Bode and Nyquist plot of $G_{\mathrm{vd}}(s)$ buck DC–DC load converter with and without filter

paper reports the usefulness of the suggested dcμG control method.

Acknowledgements This proposed dcμG model simulation was supported by the OPAL-RT Technologies India PVT LTD (North and East India). The authors thank Gagan Deep Singh Puri, a Sales Manager, for his support for providing real-time simulator device.

References

1. Kumar, M.; Srivastava, S.C.; Singh, S.N.: Control strategies of a DC microgrid for grid connected and islanded operations. IEEE Trans. Smart Grid **6**(4), 1588–1601 (2015)
2. Jadav, A.; Karkar, H.M.; Trivedi, I.N.: A Review of microgrid architectures and control strategy. J. Inst. Eng. Ser. B **98**(6), 591–598 (2017)
3. Jin, Z.; Sulligoi, G.; Cuzner, R.; Meng, L.; Vasquez, J.C.; Guerrero, J.M.: Next-generation shipboard DC power system: introduction smart grid and dc microgrid technologies into maritime electrical netowrks. IEEE Electrification Mag. **4**(2), 45–57 (2016)
4. Liu, N.; Wang, J.; Wang, L.: Distributed energy management for interconnected operation of combined heat and power-based microgrids with demand response. J. Mod. Power Syst. Clean Energy **5**, 478 (2017)
5. Adhikari, S.; Xu, Q.; Tang, Y.; et al.: Decentralized control of two DC microgrids interconnected with tie-line. J. Mod. Power Syst. Clean Energy **5**, 599 (2017)
6. Bouzid, A.M.; Guerrero, J.M.; Cheriti, A.; Bouhamida, M.; Sicard, P.; Benghanem, M.: A survey on control of electric power distributed generation systems for microgrid applications. Renew. Sustain. Energy Rev. **44**, 751–766 (2015)
7. Lotfi, H.; Khodaei, A.: AC versus DC microgrid planning. IEEE Trans. Smart Grid **8**(1), 296–304 (2017)
8. Sanjeev, P.; Padhy, N.P.; Agarwal, P.: Peak energy management using renewable integrated DC microgrid. IEEE Trans. Smart Grid **9**(5), 4906–4917 (2018)
9. Shivam,; Dahiya, R.: Intelligent distributed control techniques for effective current sharing and voltage regulation in DC distributed systems. Arab. J. Sci. Eng. **42**, 5071 (2017)
10. Wu, D.; Tang, F.; Dragicevic, T.; Vasquez, J.C.; Guerrero, J.M.: A control architecture to coordinate renewable energy sources and energy storage systems in islanded microgrids. IEEE Trans. Smart Grid **6**(3), 1156–1166 (2015)
11. Li, X.; et al.: Flexible interlinking and coordinated power control of multiple DC microgrids clusters. IEEE Trans. Sustain. Energy **9**(2), 904–915 (2018)
12. Moayedi, S.; Davoudi, A.: distributed tertiary control of DC microgrid clusters. IEEE Trans. Power Electron. **31**(2), 1717–1733 (2016)

13. Meng, L.; Dragicevic, T.; Roldán-Pérez, J.; Vasquez, J.C.; Guerrero, J.M.: Modeling and sensitivity study of consensus algorithm-based distributed hierarchical control for DC microgrids. IEEE Trans. Smart Grid **7**(3), 1504–1515 (2016)
14. Moayedi, S.; Davoudi, A.: Cooperative power management in DC microgrid clusters. In: 2015 IEEE 1st International Conference on Direct Current Microgrids, ICDCM 2015, pp. 75–80 (2015)
15. Che, L.; Shahidehpour, M.; Alabdulwahab, A.; Al-Turki, Y.: Hierarchical coordination of a community microgrid with AC and DC microgrids. IEEE Trans. Smart Grid **6**(6), 3042–3051 (2015)
16. Singh, S.N.; Srivastava, S.C.; Kumar, M.; Ramamoorty, M.: Development of a control strategy for interconnection of islanded direct current microgrids. IET Renew. Power Gener. **9**(3), 284–296 (2015)
17. Peyghami, S.; Mokhtari, H.; Blaabjerg, F.: Decentralized load sharing in a low-voltage direct current microgrid with an adaptive droop approach based on a superimposed frequency. IEEE J. Emerg. Sel. Top. Power Electron. **5**(3), 1205–1215 (2017)
18. Shuai, Z.; Mo, S.; Wang, J.; et al.: Droop control method for load share and voltage regulation in high-voltage microgrids. J. Mod. Power Syst. Clean Energy **4**, 76 (2016)
19. García, P.; Arboleya, P.; Mohamed, B.; Vega, A.A.C.; Vega, M.C.: Implementation of a hybrid distributed/centralized real-time monitoring system for a DC/AC microgrid with energy storage capabilities. IEEE Trans. Ind. Inform. **12**(5), 1900–1909 (2016)
20. Federico, I.; Jose, E.; Luis, F.: Master–slave DC droop control for paralleling auxiliary DC/DC converters in electric bus applications. IET Power Electron. **10**(10), 1156–1164 (2017)
21. Tani, A.; Camara, M.B.; Dakyo, B.: Energy management in the decentralized generation systems based on renewable energy—ultracapacitors and battery to compensate the wind/load power fluctuations. IEEE Trans. Ind. Appl. **51**(2), 1817–1827 (2015)
22. Xu, Q.; et al.: A decentralized dynamic power sharing strategy for hybrid energy storage system in autonomous DC microgrid. IEEE Trans. Ind. Electron. **64**(7), 5930–5941 (2017)
23. Liserre, M.; Blaabjerg, F.; Hansen, S.: Design and control of an LCL-filter-based three-phase active rectifier. IEEE Trans. Ind. Appl. **41**(5), 1281–1291 (2005)
24. Wu, B.; Lang, Y.; Zargari, N.; Kouro, S.: Power Converters in Wind Energy Conversion Systems: Power Conversion and Control of Wind Energy Systems, vol. 76, ch. 4, 1st edn, pp. 164–175. Wiley (2011)
25. Elgendy, M.A.; Zahawi, B.; Atkinson, D.J.: Assessment of perturb and observe MPPT algorithm implementation techniques for PV pumping applications. IEEE Trans. Sus. Energy **3**(1), 21–33 (2012)
26. Prasad, J.S.; Bhavsar, T.; Ghosh, R.; Narayanan, G.: Vector control of three-phase AC/DC front-end-converter. Sadhana **33**(5), 591–613 (2008)
27. Kaura, V.; Blasko, V.: Operation of a phase locked loop system under distorted utility conditions. IEEE Trans. Ind. Appl. **33**(1), 58–63 (1997)
28. Sun, K.; Zhang, L.; Xing, Y.; Guerrero, J.M.: A distributed control strategy based on DC bus signaling for modular photovoltaic generation systems with battery energy storage. IEEE Trans. Power Electron. **26**(10), 3032–3045 (2011)
29. Zhi, N.; Zhang, H.; Xiao, X.: Switching system stability analysis of DC microgrids with DBS control. In: 2016 IEEE Applied Power Electronics Conference and Exposition (APEC), Long Beach, CA, pp. 3338–3345 (2016)
30. Tahim, A.P.N.; Pagano, D.J.; Lenz, E.; Stramosk, V.: Modeling and stability analysis of islanded DC microgrids under droop control. IEEE Trans. Power Electron. **30**(8), 4597–4607 (2015)
31. Erickson, R.W.: Input Filter Design: Fundamentals of Power Electronics, vol. 1, ch. 10, 1st edn, pp. 378–408. Springer (1997)
32. Iftikhar, M.U.; Sadarnac, D.; Karimi, C.: Input filter damping design for control loop stability of DC-DC converters. In: IEEE International Symposium on Industrial Electronics, pp. 353–358 (2007)
33. Yoo, C.; Choi, W.; Chung, I.; Won, D.; Hong, S.; Jang, B.: Hardware-in-the-loop simulation of DC microgrid with multi-agent system for emergency demand response. In: 2012 IEEE Power and Energy Society General Meeting, San Diego, CA, pp. 1–6 (2012)
34. OPAL-RT Technologies, Presented at Online Brochure available at: http://www.OpAL-RT.com. Accessed 20 Nov 2018